Monte Carlo multiple-scattering simulation and data correction in small-angle static light scattering

Luca Cipelletti*
Dipartimento di Fisica and Istituto Nazionale per la Fisica della Materia, Università di Milano, Via Celoria 16, 20133 Milano, Italy
(Received 6 December 1996)

Monte Carlo methods usually employed for γ- and x-ray problems have recently been utilized for simulating multiple Rayleigh light scattering to all orders. Here a technique is discussed to separate the two-dimensional problem of generating the polar and azimuthal scattering angles into two independent one-dimensional samplings, thus increasing the computational efficiency. Although the method has quite a general applicability, this paper is focused on small-angle light-scattering simulations, and an artifice is introduced which reduces the inherent poor efficiency of the polar angle sampling in conjunction with differential scattering cross sections that are sharply peaked in the forward direction. As a test, the technique was used to correct two sets of experimental data affected by multiple scattering. Microporous membrane filters under quasi-index-matching conditions were investigated, and two stacks of different thickness were used. While the raw data are of course appreciably different for different sample thicknesses, the corrected scattered intensity distributions are the same, thus providing evidence of the method effectiveness in retrieving the single-scattered intensity distributions. [S1063-651X(97)09806-1]

PACS number(s): 02.70.Lq, 42.25.Fx, 61.43.Gt, 61.43.Hv

I. INTRODUCTION

Multiple scattering is a quite general physical process that inevitably occurs when a wave propagates in a strongly scattering medium, and it severely distorts the singly scattered intensity angular distribution. Since single-scattering processes are the only ones which can be easily interpreted, a data correction procedure is highly desirable to exploit light scattering fully.

Data correction is usually based on a Monte Carlo simulation of the propagation of a large number of photons in the sample. This approach has been used since the 1970s to study the effect of multiple Compton and Rayleigh x- and γ-ray scattering [1–5]. More recently, Bailey and Cannell applied a similar technique to calculate multiple scattering in static light-scattering experiments [6], overcoming simulation difficulties due to the imaging geometry that is often used in light scattering setups.

Data correction for the multiple scattering is usually accomplished by iteratively running the simulation program [1,3,6]. One starts with a reasonable guess of the singly scattered intensity to obtain the simulated total (single plus multiple) scattered intensity. The initial estimate is then refined by comparing the result of the simulation with the experimental data, and a corrected version is used as an input for a second run. The entire process is repeated until the simulated scattered intensity converges to the experimental data. It is to be noticed that an *a priori* knowledge of the functional form of the single-scattering distribution is of great help in the correction procedure, even if it is not strictly necessary.

The most difficult task in a Monte Carlo simulation is the two-dimensional problem of generating the polar and azimuthal scattering angles according to the appropriate probability density function (PDF). It is required that the sampling algorithm should be fast, to make the simulation time reasonable, and also flexible, so that various differential scattering cross sections may be simulated. Bailey and Cannell [6] proposed a quite general method, which consists of the binning of the whole solid angle in a way such that the scattering probability per bin is the same. At each scattering a new propagation direction is chosen at random among all the bins. Although their method proved to be highly efficient in various scattering geometries, it is unfortunately difficult to apply in the case of very low-angle scattering experiment simulations. In fact, to avoid any quantization distortions it is necessary that the typical bin extension be much smaller than the intensity angular distribution scale of variation, which is usually very small for low-angle experiments. Since even for low-angle simulations the binning of the entire solid angle is needed, it follows that an exceedingly large number of bins would be required to achieve the desired angular resolution. Recently, there has been a growing interest in the extremely low-angle scattering machines, which can cover now angles as low as 0.01° [7]. Such machines are designed to investigate scatterers larger than those studied with conventional setups. Large turbidities are easily encountered, and a data correction procedure which efficiently tackles the difficulties posed by low-angle scattering simulations is therefore needed.

The main purpose of this paper is to present a Monte Carlo simulation procedure based on the separation of the two-dimensional angular sampling into two one-dimensional PDF samplings. Since a one-dimensional sampling algorithm is much faster than a two-dimensional one, this method results in a fast simulation of photon propagation for any isotropic scattering system, where the scattering depends only on the magnitude of the scattering wave vector. Moreover, the technique may be also applied to γ- and x-ray scattering and to any scattering geometry, and it is particularly well suited for small-angle light-scattering experiment simula-

*Electronic address: cipelletti@mi.infn.it

tions. For these cases, the polar angle sampling algorithm efficiency is usually limited by the sharply peaked shape of the polar PDF. A simple artifice will be described, which allows a much more efficient sampling, increasing the simulation speed by a factor as large as 5.

An application to the correction of scattering data from microporous membrane filters permeated by a quasi-index-matching solvent will also be presented. It is to be pointed out that, for this system, the single-scattered intensity distribution functional form is not known *a priori*, thus making the correction procedure test a particularly severe one. Not only does the data correction turn out to be self-consistent since the process converges, but it also yields the same result for samples of different thickness—and therefore different amount of multiple scattering—thus providing a good test of the effectiveness of the method.

The paper is organized as follows: Sec. II briefly describes a typical small-angle light-scattering experimental setup. The Monte Carlo simulation is presented in Sec. III, particular emphasis being given to the angular sampling technique. Finally, Sec. IV is devoted to an application of the multiple-scattering correction procedure to scattering data from two samples (microporous membrane filters) of the same kind but with different thickness.

II. SMALL-ANGLE EXPERIMENTAL SETUP

In this section a typical small-angle static light-scattering apparatus will be briefly described, and I will focus on those details that are more important in view of the Monte Carlo simulation. As a characteristic example of the optical arrangement, I will refer to the experimental setup described by Carpineti *et al.* [8], which was also used to take the scattering data presented in Sec. IV.

In the Carpineti *et al.* setup, a collimated laser beam falls onto a cell, and the transmitted beam, together with the scattered light, is collected by a lens L. The sensor is placed in the focal plane of L, and it consists of 31 solid state elements shaped as a quarter of annulus. On center a tiny hole allows the transmitted beam to pass clear of the sensing elements and to be detected by a photodiode placed behind the sensor. In this way, the sample transmission T may be measured by dividing the transmitted beam power in the presence of the sample by that with the cell filled with the solvent alone. It is to be pointed out that multiple scattering does not affect the measured T value, since the transmission is determined from the unscattered (transmitted) beam power [9]. The sample turbidity τ may be calculated from $\tau=-z_{\mathrm{cell}}^{-1}\ln T$, where z_{cell} is the cell optical path. Note that $l=\tau^{-1}$ is the photon mean free path.

With this optical scheme, scattered photons are collected by sensor elements at different radii according to the polar exit angle θ (scattering angle). The apparatus thus allows the collection of scattered light at 31 angles, ranging from 0.1° to 13.5°, and corresponding to almost a two-decade range in wave vector $q=4\pi n_s\lambda^{-1}\sin(\theta/2)$, where n_s is the sample refractive index and λ the vacuum wavelength. It is to be noted that the setup collects all the photons scattered from the sample, and therefore it has no rejection scheme against multiple scattering. On the other hand, the advantage of such an optical scheme is that the overall solid angle subtended by the sensor is a substantial fraction of the one in which most of the incident light is typically scattered, thus resulting in an efficient scattered light detection. The scattering experiment itself may be simulated in a very effective way. In fact, it is very unlikely that a photon, which has been propagated through the sample, exits the cell along a direction such that it is not collected by the simulated sensor. Therefore, only a negligible number of photons are to be rejected after time-consuming propagation through the cell.

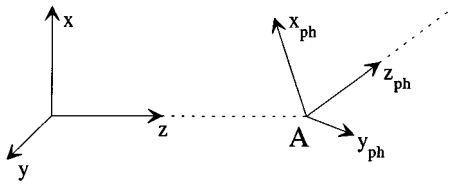

FIG. 1. The laboratory frame (x,y,z) and the photon frame $(x_{\mathrm{ph}},y_{\mathrm{ph}},z_{\mathrm{ph}})$, after scattering has occurred at point A.

III. MONTE CARLO SIMULATION

A. General scheme

We assume that the incident beam propagates along the z axis of the laboratory frame, and is linearly polarized in the x-axis direction (vertical direction). As will be seen in the following, it is also convenient to introduce a photon frame $(x_{\mathrm{ph}},y_{\mathrm{ph}},z_{\mathrm{ph}})$, where the z_{ph} axis corresponds to the photon propagation direction and the x_{ph} axis is parallel to the photon polarization (see Fig. 1). For unscattered photons, the z_{ph} and z axes coincide, while the x_{ph} and y_{ph} axes are parallel to the x and y axes, respectively. The beam is assumed to have a Gaussian profile with a beam radius w, so that the radial intensity distribution at the entrance cell wall is $I(r)=I_0\exp(-2r^2/w^2)$.

The general scheme of the Monte Carlo simulation is similar to that described in Refs. [1,6]. The path of a large number of photons is tracked through the cell by repeating, for each photon, the following steps:

(1) *Photon position at the cell entrance*. The polar coordinates (r,ϕ) in the entrance $x-y$ plane are calculated. Since the incoming beam profile is Gaussian, the probability that the radial coordinate at the cell entrance lies between r and $r+dr$ and the angular coordinate lies between ϕ and $\phi+d\phi$ is proportional to $\exp(-2r^2/w^2)r\,dr\,d\phi$. Accordingly, first ϕ is chosen at random in $(0,2\pi)$, then r is computed by sampling the PDF $(4r/w^2)\exp(-2r^2/w^2)$. This can be easily done by means of the inverse transform method [10], by choosing $r=(w/\sqrt{2})\sqrt{-\ln(1-\xi)}$ [here and in the following ξ indicates a random number uniformly distributed in (0,1)]. Finally, polar coordinates are transformed into Cartesian coordinates. If r is so large that the calculated photon position lies out of the entrance cell wall, both r and ϕ are rejected and the sampling is repeated. Note that step (1) may be skipped if the beam lateral extension can be neglected, i.e., if the difference between the width of the scattering cell and w is much larger than the photon mean free path.

(2) *First scattering event*. In order to save computing time, only scattered photons are tracked through the cell; this is obtained by forcing the first scattering event to happen

within the cell. The path d_{first} before the first scattering event is therefore calculated by sampling the exponential PDF $\tau^{-1}\exp(-\tau z)$ only for $0 \leqslant z \leqslant z_{\text{cell}}$. This is obtained by choosing $d_{\text{first}} = -\tau^{-1}\ln[1-\xi(1-T)]$.

(3) *Scattering direction*. The probability $dP(\theta,\varphi)$, that a photon is scattered within the solid angle $d\Omega$ in the direction defined by the polar angle θ, the scattering angle, and the azimuthal angle φ (with respect to the photon frame; see Fig. 2) is $dP(\theta,\varphi) \propto (d\sigma/d\Omega)d\Omega$, where $d\sigma/d\Omega$ is the single-scattering differential cross section. Accordingly, the scattering direction is calculated by sampling the bivariate angular PDF $(dP/d\theta\, d\varphi)(\theta,\varphi)$. Finally, the scattering direction is transformed back to the laboratory frame. Details on the angular sampling procedure will be given in Sec. III B.

(4) *Distance before the next scattering event*. The photon is propagated along the direction calculated at point (3) until it is scattered once more. The distance d traveled before the next scattering event is sampled from the exponential PDF $\tau^{-1}\exp(-\tau z)$, so that $d = -\tau^{-1}\ln(1-\xi)$. The distance d_{cell} from the last scattering event to the cell wall along the propagation direction calculated at point (3) is also computed.

Points (3) and (4) are repeated until photon exits from the cell, i.e., until the distance to the next scattering as calculated at point (4) would be greater than the distance to the cell wall $(d > d_{\text{cell}})$.

(5) *Photon counting*. In the optical geometry of a typical small-angle light-scattering (SALS) instrument, each detector element corresponds to a different photon exit angular range. When a photon exits from the cell, an index variable associated with the proper sensor element is updated, in order to accumulate the number of photons detected by each of the 31 channels.

The number of launched photons must be large enough to achieve a good statistics for all detector channels. At the end of the run, the number of recorded counts is normalized in order to obtain the simulated total scattered intensity $I_t(q_i)$ $(i = 1,2,\ldots,31)$. For each channel, the normalization factor accounts for the solid angle subtended by the related detector element and for the fact that photons are detected even out of the scattering plane [the (y,z) plane in the laboratory frame]. It is to be pointed out that $I_t(q_i)$ depends on the total number of tracked photons. In order to compare $I_t(q_i)$ with the experimentally measured scattered intensity $I_{\text{expt}}(q_i)$, the simulation data are therefore multiplied by a factor M chosen in such a way that the total simulated and measured scattered power are the same. This is done by taking $M = [\int d\Omega I_{\text{expt}}(q)\sin^2\psi]/[\int d\Omega I_t(q)\sin^2\psi]$, where $I_{\text{expt}}(q)$ and $I_t(q)$ are fits of the measured and simulated data, respectively, and ψ is the angle between the incident polarization vector and the scattered propagation vector (see Fig. 2). Track is also kept of the number of scattering events which each photon undergoes, so that the contribution of single-, double-, and higher-order scattering to the overall scattered intensity may be monitored.

B. Angular sampling

The angular PDF to be sampled is $(dP/d\theta\, d\varphi)(\theta,\varphi) = N/\pi I(q(\theta))\sin\theta\sin^2\psi \equiv \Sigma(\theta,\varphi)$, where I is the singly scattered light intensity distribution and N/π is a normalizing factor, so that $\int_0^{2\pi} d\varphi \int_0^{\pi} d\theta\, \Sigma(\theta,\varphi) = 1$ (see Fig. 2 for a sketch of the θ, φ, and ψ angles). It is to be emphasized that Σ is a function of the two random variables θ and φ, which are not separable, due to the dipole factor $\sin^2\psi$. In fact, $\sin^2\psi = 1-\cos^2\psi = 1-\sin^2\theta\cos^2\varphi$ and Σ cannot be factored in a θ-dependent term times a φ-dependent term, as would be required for θ and φ to be random independent variables [10]. In order to design a fast and flexible algorithm for sampling Σ, it is, however, desirable to sample the angular variables θ and φ separately. The task is then split into the easier and faster independent sampling of a PDF for φ—the same for every scattering system—and of a PDF for θ, which contains information on the specific scattering system through $I(q)$. To do that, one takes advantage of the trigonometric identities $\sin^2\psi = 1-\cos^2\psi = 1-\sin^2\theta\cos^2\varphi = \sin^2\varphi + \cos^2\varphi\cos^2\theta$ to rewrite the angular PDF in the form

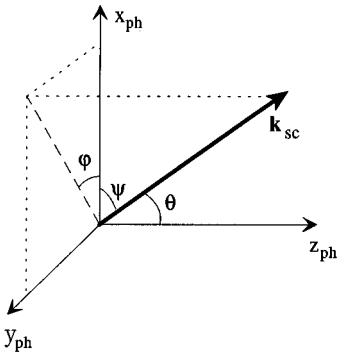

FIG. 2. Relevant angles in the scattering, with respect to the photon frame: θ is the (polar) scattering angle, φ the azimuthal scattering angle, and ψ is the angle between incoming photon polarization and scattered photon propagation direction $\mathbf{k}_{\text{sc}}$.

$$\Sigma(\theta,\varphi) = \beta_1 g_1(\theta,\varphi) + \beta_2 g_2(\theta,\varphi), \tag{1}$$

where

$$\beta_1 = \int_0^{\pi} d\theta\, NI(q(\theta))\sin\theta, \tag{2a}$$

$$g_1(\theta,\varphi) = \frac{N}{\beta_1} I(q(\theta))\sin\theta\,\frac{\sin^2\varphi}{\pi}, \tag{2b}$$

$$\beta_2 = \int_0^{\pi} d\theta\, NI(q(\theta))\sin\theta\cos^2\theta, \tag{3a}$$

$$g_2(\theta,\varphi) = \frac{N}{\beta_2} I(q(\theta))\sin\theta\cos^2\theta\,\frac{\cos^2\varphi}{\pi}. \tag{3b}$$

As both g_1 and g_2 are positive, and $\beta_1+\beta_2 = 1$, the composition method [10] may be applied to sample Σ. Accordingly, g_1 is sampled with probability β_1 and g_2 with probability β_2; that is, one generates ξ and sample g_1 if $\xi < \beta_1$, and g_2 otherwise. Moreover, both g_1 and g_2 are the products of a θ-dependent factor and a φ-dependent factor. Therefore, the two angular variables are independent random variables [10], and the most convenient sampling method may be separately applied to each of them.

Let me first consider the rather straightforward sampling of the φ-dependent terms in Eqs. (2b) and (3b), focusing my attention only on the $\sin^2\varphi/\pi \equiv \Phi(\varphi)$ factor in Eq. (2b), since

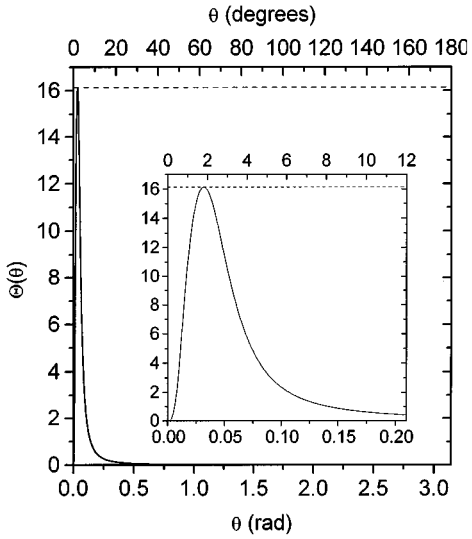

FIG. 3. A typical $\Theta(\theta)$ for small-angle light scattering (see text for more details). Note the sharp peak in the very low-angle region, zoomed in the inset. The dashed line is the upper limiting function $y=\Theta_{\max}$ used in the acceptance-rejection algorithm for the sampling.

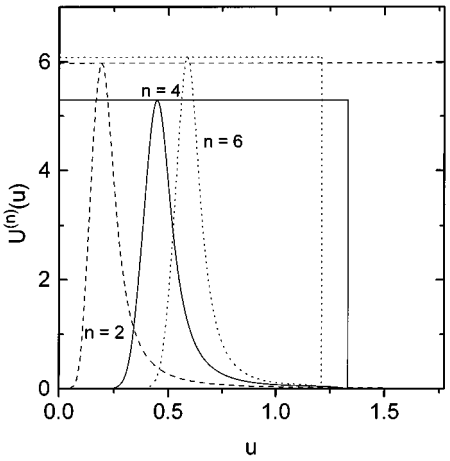

FIG. 4. Probability density function $U^{(n)}(u)$ and related upper limiting function for various n (see the text for the definition). The plotted functions correspond to the case shown in Fig. 3.

the sampling of the analogous φ dependent factor in Eq. (3b) may be simply obtained from the sampling of $\Phi(\varphi)$. In fact, one notices that if φ is a random angle in $(0,2\pi)$ with PDF $\Phi(\varphi)$, then $\varphi'=[(\varphi+\pi/2)\mathrm{mod}2\pi]$ is a random angle in $(0,2\pi)$ with PDF $\cos^2\varphi/\pi$ (a mod b indicates the remainder of the division a/b). Since $\Phi(\varphi)$ is periodic with period π, to sample it one generates φ from $\Phi(\varphi)$ for $0\leqslant\varphi<\pi$ and adds π to the result, with probability $\frac{1}{2}$. This can be done quite efficiently by means of a combination of the inverse transform and acceptance-rejection methods [10]. Using $\sin\varphi/\pi$ as an upper limiting function for $\Phi(\varphi)$, one first takes $\varphi=\arccos(1-2\xi)$ (the inverse transform method), and then accepts φ with probability $\sin^2\varphi/\sin\varphi$ (acceptance-rejection method).

I turn now to a discussion of the sampling of the θ-dependent factors in Eqs. (2b) and (3b), which depend on the particular scattering system through the single-scattering intensity $I(q)$. Accordingly, the sampling algorithm must be flexibly designed, since different functional forms may be used. Either the numerical inverse transform method [11] or the acceptance-rejection method are suitable. The former consists in numerically dividing $(0,\pi)$ into a large number of tiny intervals, such that the probability of the scattering angle to lie in each interval is the same. Prior to the simulation run, a reference table is built up, containing the center of all intervals, and it is stored in the computer memory. At each scattering event, θ is chosen at random among the angles listed in the reference table. This scheme has the advantage of allowing a fast sampling of the θ PDF, once the reference table has been built. However, it suffers from the fact that building and storing the reference table is time and memory consuming, especially for very low-angle light-scattering simulations, where a large number of tiny intervals are required. In fact, to avoid distortions due to the quantization of the scattering angles, the average interval width has to be much smaller than both the typical scale of variation of $I(q)$ and the sensor element angular spacing. In contrast, the acceptance-rejection algorithm does not need any prior reference table building, and it generates a continuous distribution of scattering angles, thus avoiding any quantization effects. However, the generation of θ at each scattering event is slower than in the previous case. I implemented both algorithms and, for a typical simulation run where 10^6 photons are launched, the overall computing time is quite similar. Since the acceptance-rejection method is more easy to program, I will describe it, referring for simplicity only to g_1: a similar procedure is needed for sampling g_2.

Let $\Theta(\theta)=N_1 I(q(\theta))\sin\theta$ be the θ-dependent factor of $g_1(\theta,\varphi)$, normalized so that $\int_0^\pi d\theta\,\Theta(\theta)=1$, and let $\Theta_{\max}$ be the maximum of $\Theta(\theta)$ in $(0,\pi)$. The acceptance-rejection algorithm is implemented with $y(\theta)=\mathrm{const}=\Theta_{\max}$, $0\leqslant\theta\leqslant\pi$, as an upper limiting function for $\Theta(\theta)$. At each scattering event the scattering angle is therefore chosen at random in $(0,\pi)$, by taking $\theta=\xi\pi$. Finally, θ is accepted with probability $\Theta(\theta)/\Theta_{\max}$. As is known, the efficiency of the algorithm—i.e., the probability P_θ of θ to be accepted once it has been generated—is given by the ratio of the area under $\Theta(\theta)$ to the area under $y(\theta)$ (see Fig. 3):

$$P_0=\frac{\int_0^\pi d\theta\,\Theta(\theta)}{\int_0^\pi d\theta\,y(\theta)}=\frac{1}{\pi\Theta_{\max}}. \tag{4}$$

A typical $\Theta(\theta)$ for SALS is shown in Fig. 3 together with the corresponding $y(\theta)$: the presence of a very sharp peak near $\theta=0$ (see the inset) is due to the $\sin\theta$ factor combined with the fact that most of the light is scattered at very low angles [12].

It is clear that a very low-P_θ value corresponds to such a shape, thus making the acception-rejection algorithm a rather slow one. Consequently, one would desire to generate the scattering angle by sampling a much less peaked PDF. This can be accomplished by the following artifice: instead of directly sampling $\Theta(\theta)$, one chooses $\theta=u^n$, where u is a random variable with (properly normalized) PDF $U^{(n)}(u)=n\Theta(u^n)u^{n-1}$, $0\leqslant u\leqslant\sqrt[n]{\pi}$ [13], and $U^{(n)}$ is sampled by means of the acceptance-rejection method as described above. Fig. 4 shows $U^{(n)}(u)$ for various n for the same $\Theta(\theta)$

as in Fig. 3. The correspondent upper limiting functions are also shown. Note that all curves are much less peaked, and that the areas under the upper limiting functions are definitely smaller than in the previous case, thus resulting in a greater computational efficiency, as defined analogously to Eq. (4). For the case shown in Figs. 3 and 4, the acceptance is maximized for $n=4$, P_θ being 0.14, a much larger value compared with $P_\theta=0.02$, which holds for the direct sampling of $\Theta(\theta)$. By using this artifice, the overall simulation time is typically reduced by a factor as large as 5. Finally, it is to be pointed out that this method proves to be useful also if the numerical inverse transform technique is chosen to sample $\Theta(\theta)$, since it drastically reduces the time required to build up the angular reference table.

C. Experimental data correction procedure

The Monte Carlo simulation described in the previous sections may be applied to the correction of experimental scattering data, as I will now explain. An iterative scheme is used [1,3,6] to improve an initial guess $I_s^{(0)}$ of I_s, the unknown single-scattering distribution. A function obtained by fitting $I_s^{(0)}$ is input to the Monte Carlo code to obtain the first-order simulated total scattered intensity $I_t^{(1)}$, where the superscript refers to the number of iterations. $I_t^{(1)}$ is compared with the experimental scattered intensity I_t^{expt} to calculate a more refined guess of the single-scattered intensity, which in turn may be fitted and used as the input to the second iteration, and so forth. After n iterations, the correction of the single scattering guess is done by taking

$$I_s^{(n)}=I_s^{(n-1)}\,\frac{I_t^{\text{expt}}}{I_t^{(n)}}. \tag{5}$$

The iterative procedure is carried on until the simulated total scattered intensity agrees with the experimental scattered intensity within a fixed error, typically a few percent. Note from Eq. (5) that, as the simulated scattered intensity approaches the experimental data, the single-scattering guess calculated at successive runs changes only slightly, eventually converging to the single-scattering intensity I_s.

An important point in applying the data correction scheme to small-angle scattering experiments is that the data are usually available only in a limited angular range, while the simulation requires a guess of the single scattering over the whole range of wave vectors. In practice, however, data correction turns out to be feasible, provided that most of the scattered light I_t^{expt} falls within the angular range spanned by the sensor, and that one can extrapolate in a sensible way the high-q behavior from the available data.

IV. APPLICATION

The multiple-scattering data correction procedure has been tested by applying it to the scattered intensity distributions from two samples of the same kind, but with different thicknesses. If multiple scattering were not present, one would expect the scattered intensity distributions of the two samples to be simply proportional. Of course, multiple scattering will cause the intensity distributions to be different. By contrast, as it will be shown in the following, the corrected intensity distributions (i.e., the reconstructed single-scattering distributions) are proportional within the experimental errors, thus providing evidence of the effectiveness of the correction process.

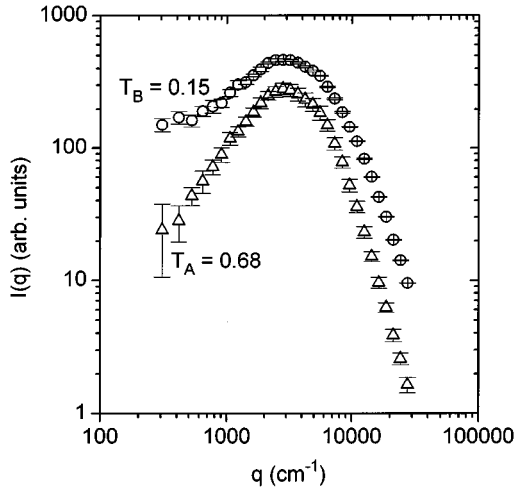

FIG. 5. Experimental scattered intensity distribution for two samples of the same material (acetate of cellulose microporous membrane filters) but with different thickness. Open triangles refer to sample A, open circles to sample B, five times thicker than sample A. Curves are labeled by the sample transmission value.

The samples are microporous membrane filters (Sartorius SM 123 03) made of acetate of cellulose and permeated by a quasi-index-matching solvent, *p*-cymene [14]. These membranes are highly porous, the pore boundary having fractal morphology, and their spatial structure exhibits a quasiperiodicity over a typical length of approximately 10 μm. Due to these features, their scattered intensity distribution is peaked at a very low wave vector, and it steeply decays at larger q following a power law. The ''thin'' sample, which will be labeled as sample A, is a single membrane, while sample B, the ''thick'' one, is made up by a stack of five membranes. All the membranes were measured to have equal thickness (140 ± 5 μm) and the scattered intensity distribution of each of them was checked to be the same within the experimental errors.

Figure 5 shows the experimental scattered intensity distributions I_{A} and I_{B} for samples A and B. The measured transmission for the two samples are $T_{\text{A}}=0.68$, corresponding to a photon mean free path $l=363\pm13$ μm, and $T_{\text{B}}=0.15$, corresponding to $l=369\pm13$ μm. It should be noted that the l values calculated for the two samples from the transmission and thickness data are in good agreement. The photon mean free path is definitely larger than the thickness of sample A (140 μm), and approximately half the thickness of sample B (700 μm). Accordingly, one expects multiple-scattering contributions to be much more relevant for sample B than for sample A. The presence of multiple scattering to an extent which is different for the two samples is confirmed by the fact that the shape of I_{A} and I_{B} in a log-log plot is not the same (see Fig. 5).

The experimental data of both samples were corrected for multiple scattering, as explained in Sec. III. The single-scattering cross-section functional form being unknown, the data were fitted with a quite general function, namely, the ratio of two polynomials, the numerator and denominator degree being 3 and 7, respectively. This functional form

proved to fit accurately both the experimental scattering data and the estimated single scattering profile calculated at the end of each iteration. The extrapolation of the fitting function out of the experimentally accessible q range provides a physically reasonable behavior of the scattered intensity, by following the same steep power-law decay observed in the fitting range for the larger wave vectors. The choice of a physically reasonable scattering profile was also eased by the fact that the membrane filters scatter substantially only within a narrow lobe in the forward direction. In fact, by integrating the experimental data fitting function, one can estimate that more than 90% of the light scattered by the sample actually falls in the q range covered by the instrument sensor.

Typically 2–4 iterations were necessary for the correction process to converge. In each computer run 10^6 scattered photons were tracked through the sample, the resulting statistical fluctuation for each detector sensing element being less than the correspondent experimental error. The computing time for a single run was approximately 3–6 min on a VAX 7000/610 computer, depending on the sample thickness. The program was also run on a Intel Pentium 120-MHz based personal computer (PC), and on an Intel 486 DX2 66-MHz based PC. In the former case the computing time was almost the same as required by the VAX, while in the latter it was greater by a factor of 3.

In Fig. 6 both the experimental and the corrected scattering data of sample B are plotted. As can be noted, the effect of multiple scattering is to smear the intensity distribution, by removing scattered light from the peak in favor of the low-intensity tails at lower and higher wave vectors. This can be intuitively understood by the following balance argument. For simplicity, let me consider only double scattering within the scattering plane, corresponding to an azimuthal scattering angle $\varphi=\pi/2$. The probability that a photon—which was first scattered in the direction of the peak—undergoes a second scattering, finally exiting the sample with a different polar angle θ, is the same as the probability that a photon first scattered at θ is rescattered so that it exits in the direction of the peak, θ_{peak}. For both photons, in fact, the second scattering angle is the same, namely, $\theta_{\mathrm{peak}}-\theta$. As a consequence, the number of photons following the former scattering sequence is greater than that of the photons undergoing the latter, since the amount of photons first scattered in the peak direction is maximum. Similar arguments may also be applied out of the scattering plane and to multiple scattering of higher orders, so that the multiply scattered light displaced from the peak to the tails of the intensity distribution is not balanced from the opposite contribution. The net result of multiple scattering is therefore to flatten $I(q)$. It should be noted that the correction may be as large as a factor of 10, as observed at the lower q values in Fig. 6. High correction factors were also observed by Bailey and Cannell in the analysis of scattering data taken during the spinodal decomposition of a binary mixture at the critical concentration [6]. Qualitatively similar results were obtained when correcting the experimental data of sample A, the difference between experimental and corrected data being much less pronounced due to the reduced importance of multiple scattering in the thinner sample.

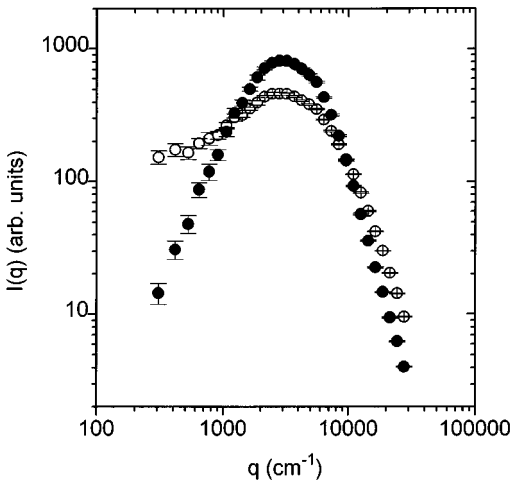

FIG. 6. Scattered intensity vs q for sample B (sample thickness 700 μm, transmission 0.15). Open circles are experimental data, filled circles are the same data after correction for multiple scattering.

An effect which is usually associated with Rayleigh scattering is the depolarization of the multiply scattered light. During the simulation, the photon polarization is tracked and therefore the depolarization ratio $I_{\mathrm{VH}}/I_{\mathrm{VV}}$ can be calculated (I_{VH} and I_{VV} are the intensity of the horizontally and vertically polarized components of the light scattered in the scattering plane, respectively). For sample B, the calculated depolarization is negligible, $I_{\mathrm{VH}}/I_{\mathrm{VV}}$ being less than 2×10^{-5} at all detected scattering angles, in spite of the large amount of multiple scattering. Such a low value is due to the very peculiar shape of the differential scattering cross section, which is sharply peaked in the forward direction, as discussed above. As a consequence, it is very unlikely that a photon is scattered out of the scattering plane by an angle greater than a few degrees. This applies to multiply scattered photons as well, the calculated average number of scattering events being of the order of 2–3. Since a significant change in the polarization direction occurs only at fairly large scattering angles and for photon propagation directions well out of the scattering plane, it follows that no appreciable depolarization is expected in the present case.

Figure 7 shows the corrected data for both samples. The shape of the two curves in a log-log plot is fairly similar, thus indicating that multiple-scattering distortions were successfully corrected (compare with Fig. 5). In order to assess more quantitatively the effectiveness of the method, in Fig. 8 I plot the ratio $I_{\mathrm{B}}/I_{\mathrm{A}}$ for both experimental and corrected data. As discussed above, if multiple scattering were not present $I_{\mathrm{B}}/I_{\mathrm{A}}$ would be constant. More precisely, it is easy to show that for all wave vectors the ratio of the scattered intensities would be equal to the ratio of the samples attenuation $1-T$ [15]: $I_{\mathrm{B}}/I_{\mathrm{A}}=(1-T_{\mathrm{B}})/(1-T_{\mathrm{A}})=2.7$. As can be seen, $I_{\mathrm{B}}/I_{\mathrm{A}}$ for the experimental data is not constant, and the behavior of the intensities ratio reflects the fact that multiple scattering displaces scattered power from the peak to lower and higher wave vectors. In contrast, the corrected data are in good agreement with the predicted value $I_{\mathrm{B}}/I_{\mathrm{A}}=2.7$, indicated by the straight line in Fig. 8. Small deviations are observed only in the small-q regime, where multiple-

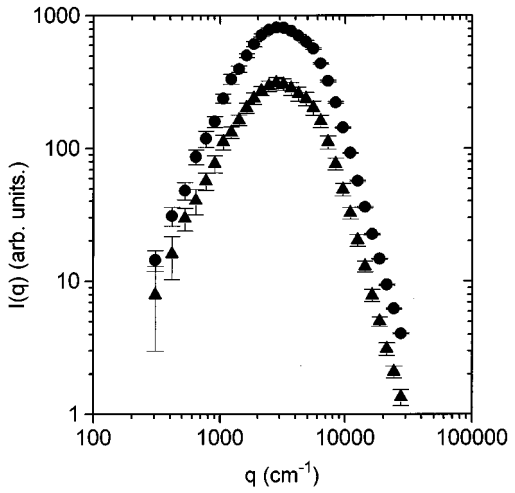

FIG. 7. Scattered intensity distribution for samples A (filled triangles) and B (filled circles), after the correction procedure. Note that the curves have fairly the same shape on a log-log plot, thus indicating that multiple-scattering effects have been successfully corrected.

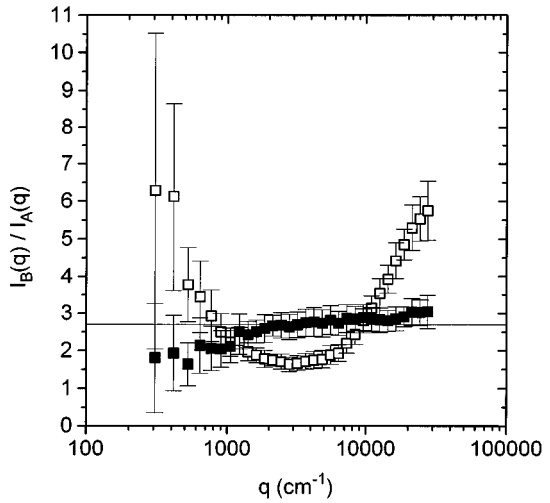

FIG. 8. Ratio of the intensity scattered by the two samples, calculated from the experimental data (open squares) and after multiple-scattering correction (filled squares). The corrected data are in good agreement with the sample attenuation ratio $(1-T_B)/(1-T_A)=2.7$, represented by the solid line, as one should expect if multiple-scattering effects were actually corrected for.

scattering effects seem to have been slightly overestimated in the correction process.

V. SUMMARY

An implementation of a Monte Carlo simulation of Rayleigh light multiple scattering to all orders has been described. The simulation is based on the propagation of a large number of photons through the sample. The most interesting feature is a technique to separate the two-dimensional problem of generating the polar and azimuthal scattering angles into two independent one-dimensional PDF samplings. The resulting azimuthal angle PDF is independent of the scattering system, and its sampling is quite straightforward. Information on the particular differential scattering cross section is embedded in the polar angle PDF. Accordingly, the θ sampling algorithm has been designed so that different scattering systems can be considered.

This scheme may also be applied to γ- and x-ray scattering, and is well suited for various scattering geometries. In particular, it allows us to overcome some difficulties posed by low-angle scattering experiment simulations, where a very high angular sampling resolution is needed to avoid quantization distortions. An artifice has been proposed to enhance the speed of the polar angle sampling, which typically is limited by the sharply peaked shape of the polar PDF. As a final remark, the simulation does not need a large computer memory, so that it may be successfully run even on a small PC.

The application of the simulation code to the correction of scattering data from microporous membrane filters in quasi-index-matching conditions has also been presented. Two samples of the same kind, but with different thicknesses were considered. In this case both the singly scattered intensity distribution and its functional form were not known *a priori*, thus making the test of the correction procedure a particularly severe one. The data corrections turned out to be self-consistent in that the iteration process previously described converged. Moreover, it yielded the same result for samples of different thickness, and corrected data were consistent with the transmitted beam attenuation measurements, thus demonstrating the method effectiveness. The intensity distribution corrections were as high as a factor of 10, as it was the case for the low-angle data of the thick sample.

ACKNOWLEDGMENTS

The author thanks A. Bailey and D. S. Cannell for providing him with the computer code for multiple scattering simulation described in Ref. [6]. He is also indebted to M. Giglio and M. Carpineti for useful discussions and for help in preparing this manuscript. This work was supported by grants from the Ministero dell'Università e della Ricerca Scientifica e Tecnologica (MURST) and from the Comitato Nazionale Ricerche Tecnologiche e Innovazione of the Consiglio Nazionale delle Ricerche (CNR).

[1] J. Felsteiner, P. Pattison, and M. Cooper, Philos. Mag. **30**, 537 (1974).

[2] J. Felsteiner and P. Pattison, Phys. Rev. B **13**, 2702 (1976).

[3] R. Serimaa, T. Pitkäneen, S. Vahvaselkä, and T. Paakari, J. Appl. Crystallogr. **23**, 11 (1990).

[4] Y. Namito, S. Ban, and H. Hirayama, Nucl. Instrum. Methods Phys. Res. Sect. A **332**, 277 (1993).

[5] F. Bell, Nucl. Instrum. Methods Phys. Res. Sect. B **86**, 251 (1994).

[6] A. E. Bailey and D. S. Cannell, Phys. Rev. E **50**, 4853 (1994).

[7] A. Vailati and M. Giglio, Phys. Rev. Lett. **77**, 1484 (1996).

[8] M. Carpineti, F. Ferri, M. Giglio, E. Paganini, and U. Perini, Phys. Rev. A **42**, 7347 (1990).

[9] The pin hole through which the transmitted beam is collected has a finite size. By consequence, it is unavoidable that, together with the transmitted light, some scattered light is also measured by the photodiode placed behind the sensor. The resulting error in calculating the transmission was evaluated running the simulation program, and it turned out to be typically negligible.

[10] See, for example, R. Y. Rubinstein, *Simulation and the Monte Carlo Method* (Wiley, New York, 1981), Chap. 3.

[11] See, for example, M. H. Kalos and P. A. Whitlock, *Monte Carlo Methods* (Wiley, New York, 1986), Vol. 1, Chap. 3.2.

[12] The function plotted in Fig. 3 corresponds to the sample described in Sec. IV.

[13] For any θ_1 and θ_2, $0 \leqslant \theta_1 < \theta_2 < \pi$, the probability that the scattering angle θ lies in the interval $[\theta_1, \theta_2]$ is $P(\theta \in [\theta_1, \theta_2]) = \int_{\theta_1}^{\theta_2} d\theta\ \Theta(\theta)$. Changing the integration variable θ to u^n yields

$$P(\theta \in [\theta_1, \theta_2]) = \int_{\sqrt{\theta_1}}^{\sqrt{\theta_2}} du\ n u^{n-1} \Theta(u^n) = \int_{u_1 = \sqrt{\theta_1}}^{u_2 = \sqrt{\theta_2}} du\ U^{(n)}(u).$$

Therefore, if u is a random variable with PDF $U^{(n)}(u)$, $0 \leqslant u \leqslant \sqrt[n]{\pi}$, then $\theta = u^n$ is a random variable with PDF $\Theta(\theta)$, $0 \leqslant \theta \leqslant \pi$.

[14] L. Cipelletti, M. Carpineti, and M. Giglio, Langmuir **12**, 6446 (1996).

[15] The attenuation $1 - T$ is the ratio of the scattered power to the incident power, and therefore it is proportional to $\int d\Omega\ I(q) \sin^2 \psi$. If multiple scatter was not present, $I_B / I_A = C$, where C is a constant independent of q, and thus

$$(1 - T_B)/(1 - T_A) = \int d\Omega\ I_B(q) \sin^2 \psi \Big/ \int d\Omega\ I_A(q) \sin^2 \psi$$
$$= \int d\Omega\ C I_A(q) \sin^2 \psi \Big/ \int d\Omega\ I_A(q) \sin^2 \psi = C.$$